Contents lists available at GrowingScience

Engineering Solid Mechanics

homepage: www.GrowingScience.com/esm

Diffusion welding features of the dissimilar 40Cr and W6Mo5Cr4V2 steels

Ivan Nikulin[a*], Tatiana Nikulicheva[a], Alexei Vyugin[a], Oleg Ivanov[a,b*], Nikita Anosov[a], Maxim Mishunin[a], OlgaTelpova[a] and Natalia Alfimova[b]

[a]*Belgorod State University, Belgorod 394015, Russian Federation*
[b]*Belgorod State Technological University named after V.G. Shukhov, Belgorod 308012, Russia Federation*

ARTICLE INFO

Article history:
Received 15 July 2024
Accepted 19 January 2025
Available online
19 January 2025

Keywords:
Diffusion welding
Hot rolled 40Cr and W6Mo5Cr4V2 steels
Host and alloying elements
Diffusion redistribution of atoms
Welding joint
Mechanical properties

ABSTRACT

Hot rolled 40Cr and W6Mo5Cr4V2 steels were diffusion-welded by using a 4-staged process including uniaxial 50 kN compression at 1200 °C in 10^{-5} mbar vacuum with following cooling down to room temperature. Structural 40Cr and high-speed tool W6Mo5Cr4V2 steels are dissimilar, since they are different (i) in content of host Fe element and alloying Cr, W, V, Mo elements, (ii) in phase composition (40Cr steel is single-phased and W6Mo5Cr4V2 steel is multi-phased), (iii) in microstructure (homogeneous inclusions-less microstructure is characteristic for 40Cr steel, composite microstructure consisting of matrix Fe-based phase with metal (W, V, Mo) carbides is characteristic of W6Mo5Cr4V2 steel), and (iv) in grain structure (40Cr steel is coarse-grained with grain ~100 μm size and W6Mo5Cr4V2 steel is fine-grained with grain size of several μm). Phase composition, microstructure and grain structure of the steels are retained after welding. Diffusion redistribution of Fe, Cr, W, V, Mo atoms results in forming the diffusion zones with different widths (several μm for W, V and Mo, ~25 for Cr and ~15 μm for Fe). Resulting concentration Cr profiles are typical for diffusion from limited sources and could be satisfactorily described by diffusion coefficient equal to ~$1.1 \cdot 10^{-14}$ $m^2 \cdot s^{-1}$ (the coefficient is weighted over the entire temperature range from 1200 °C to room temperature). Within the diffusion Cr and Fe zones, the Vickers microhardness decreases from ~2000 HV (for W6Mo5Cr4V2 steel) to ~530 HV (for 40Cr steel). During room-temperature tensile tests, the diffusion-welded steels were always fractured not in the diffusion joint but in 40Cr steel.

1. Introduction

There are two main categories of welding methods allowing permanently connecting solid parts and forming components consisting of metal materials (Khedr et al., 2023). First of them is fusion welding based on the melting process of parent materials on facing surfaces with a filler material resulting in forming a weld bead (Vaishnavan & Jayakumar, 2021; Tümer et al., 2022). The fusion welding processes are gas welding, arc welding, and intense-energy beam welding. However, the fusion welding is usually accompanied by developing internal stresses within the weld components, distortions, microstructure changes in the welded region. Besides, associated harmful effects including flashlights, ultra-violate radiation, high temperatures, and fumes are also typical for the fusion welding (Singh et al., 2019; Anawa & Olabi, 2008). Moreover, under the diffusion welding between dissimilar metal materials, several concerns should be additionally considered including the selection of filler metals, differences in melting points and mechanical properties, and thermal expansion of the metals being welded (Harada et al., 2014; Ghosh et al., 2017).

Second category of welding methods is based on solid-state welding processes in which welding is performed through coalescence at a lesser temperature than the melting temperatures of materials being welded and without using filler metal. External pressure can be also applied during some solid-state welding processes (Akca & Gürsel, 2016; Nassiri et al., 2019; Yildirim & Kelestemur 2005). The main techniques of solid-state welding are diffusion welding or bonding, friction stir welding, forge welding, cold welding and explosion welding.

* Corresponding author. Phone: +7 4722 58 54 38, Fax: +7 4722 58 54 15
E-mail addresses: Ivanov.Oleg@bsu.edu.ru (I. Nikulin)

ISSN 2291-8752 (Online) - ISSN 2291-8744 (Print)

doi: 10.5267/j.esm.2025.1.005

The diffusion welding is promising technique allowing joining both similar and dissimilar materials [Takeda et al., 1997; Hwang et al., 2023; Sharma & Kumar Dwivedi, 2021; Li et al., 2008; Gietzelt et al., 2017; Mahoney & Bampton, 1993; Kazakov, 1985). The diffusion welding is implemented at a temperature below the melting point, T_m, of the materials being welded (usually >1/2 T_m) and under compressing pressure below those that would cause macroscopic deformation to the materials. An inert atmosphere or vacuum are usually required to protect the contacting surfaces of the welded materials from oxidation. In contrast to the fusion welding, the diffusion welding can eliminate solidification defects, such as hot cracking, gas porosity, and nonmetallic inclusions, segregation problems, distortion stresses (Coronado & Cerón, 2010; Yılmaz, 2001). However, diffusion welding requires careful surface preparation before welding, like oxide removal, degreasing, brushing, and/or sandblasting. Besides, technological equipment for the diffuse welding is usually expensive enough as compared to that for ordinary fusion welding techniques.

The diffusion welding process occurs into both metal materials being welded by thermal activate diffusion mechanisms resulting in forming a welding joint, which defines the properties of welded materials (Xiong et al., 2020; Kurt, 2007; Akhter et al., 2005; Akca, & Gursel, 2017; Wang et al., 2008; Zhang et al., 2015). The diffusion welding produces a solid-state bond between the welded materials. The diffusion welding process can be divided by three stages (Mahoney & Bampton, 1993; Tsakiris et al., 2011). At the first stage, the deformation of surface asperities is implemented through plastic flow and creep. The grain boundary diffusion of atoms to the voids and grain boundary migration take place for the second stage. Finally, the solid-state volume diffusion of atoms between the materials being welded results in completely closing the surface voids and forming near-surface diffusion zones corresponding to the welding joint (Baskutis et al., 2022).

The aim of this paper is to find and analyze the features in both diffusion welding processes between the dissimilar 40Cr and W6Mo5Cr4V2 steels and in the properties of the diffusion-welded steels. The steels are different in content of host Fe element, as well alloying W, V, Mo elements. Key mechanism of the diffusion welding between these steels is based on high-temperature solid-state redistribution atoms of these elements resulting in forming a welding joint. The W6Mo5Cr4V2 steel is a molybdenum high-speed tool steel (Chen et al., 2023; Qu et al., 2013). Owing to balanced combination of abrasion resistance, toughness and good red hardness, this steel is widely applied in the production of large, complex shape and valuable tool (e.g. twist drills, taps, milling cutters, reamers, broaches, saws, knives, cold forging die, forging tools, strip cutting machine, heading forming die). The 40Cr steel is structural steel belonging to high quality low carbon, low alloy chromium, molybdenum steel (Yao et al., 2021; Yin et al,. 2020). Owing to its good mechanical properties, this steel is widely applied in the production of important quenched and tempered mechanical parts, such as gear shaft sleeve, connecting rod, screw, inlet valve, and the mold manufacturing industry such as medium plastic mold and mold structure parts such as mold frame. The 40Cr and W6Mo5Cr4V2 steels can be applied to construct combined two-component cutting tools like drills and milling cutters consisting of the 40Cr holder and the cutting W6Mo5Cr4V2 part. To strongly and reliably joint materials of the holder and cutting part, the diffusion welding could be successfully applied (Gomez de Salazar et al., 2006).

2. Materials and Methods

Commercial hot rolled 40Cr and W6Mo5Cr4V2 steels were applied to prepare the Ø50×10 mm disks with parallel opposite surfaces. These discs were next applied for diffusion welding. The discs surfaces contacted during the diffusion welding process were first sanded using sandpaper of various grits ranging from 350 to 1000, then carefully polished by using a silica suspension and finally degreased. An Instron Universal Testing Machine (Model 3369) was applied to uniaxially compress the steels being diffusion-welded and as well to test the mechanical properties of the diffusion-welded 40Cr-W6Mo5Cr4V2 steels by recording engineering strain-stress curves. A dynamic ultra-micro hardness tester (SHIMADZU, DUH-211S) was applied to additionally test the mechanical properties of the welding joint. To determine a correct elemental composition of the 40Cr and W6Mo5Cr4V2 steels, an optical emission spectrometer FOUNDRY-MASTER OE750 was applied. To identify crystal structure and phase composition of the steels, X-Ray diffraction (XRD) analysis was performed by using a Rigaku Ultima IV diffractometer with CuK_α-radiation. The Rietveld method using the PDXL (Rigaku) software was applied to refine experimental XRD patterns. Scanning electron microscopy (SEM, a Quanta 600FEG microscope) additionally involving back-scattered electron (BSE-SEM), energy dispersive X-ray spectroscopy (EDS-SEM) and electron backscatter diffraction (EBSD-SEM) methods was applied to characterize specific features in microstructure of the 40Cr and W6Mo5Cr4V2 steels as well the welding 40Cr-W6Mo5Cr4V2 joint.

3. Results and Discussion

3.1 Characterization of the 40Cr and W6Mo5Cr4V2 steels

Elemental composition of the 40Cr and W6Mo5Cr4V2 steels, which were applied for diffusion welding, is listed in **Table 1**. Of all the elements, which are usually introduced in the steels, only 8 elements are included in the Table.

Table 1. The elemental composition of the 40Cr and W6Mo5Cr4V2 steels (wt%)

Steel	C	Si	Mn	Cr	V	Mo	W	Fe
40Cr	0.416	0.298	0.678	0.989	0.003	0.010	< 0.002	97.470
W6Mo5Cr4V2	0.883	0.339	0.370	3.940	2.000	4.626	5.967	81.170

In contrast to the 40Cr steel, the W6Mo5Cr4V2 steel contains less host Fe element, but much more alloying Cr, V, Mo and W elements. The alloying elements allow tuning the mechanical properties of the steels in desired manner. Difference in the elemental composition of the steels due to the alloying elements content results in relevant change in their phase composition. Room-temperature XRD patterns taken for the 40Cr and W6Mo5Cr4V2 steels are shown in **Figs. 1(a)** and **(b)**, respectively. According to XRD analysis, the 40Cr steel is single-phased with crystal $Im\bar{3}m$ structure and lattice parameters a=b=c=2.8668 Å. The $Im\bar{3}m$ phase is the dominant one in the W6Mo5Cr4V2 steel, too. However, a few minor phases were also observed in the XRD pattern for the W6Mo5Cr4V2 steel. These phases were identified as different metal carbides including iron tungsten carbide, vanadium carbide and molybdenum carbide. Forming the carbide phases is clearly confirmed by appearance of relevant peaks in XRD pattern, as shown in inset to **Fig. 1 (b)**. Difference between the phase composition of the 40Cr and W6Mo5Cr4V2 steels observed in XRD patterns can be also found in BSE-SEM images taken from polished surfaces of these steels (**Figs. 1 (c)** and **(d)**, respectively).

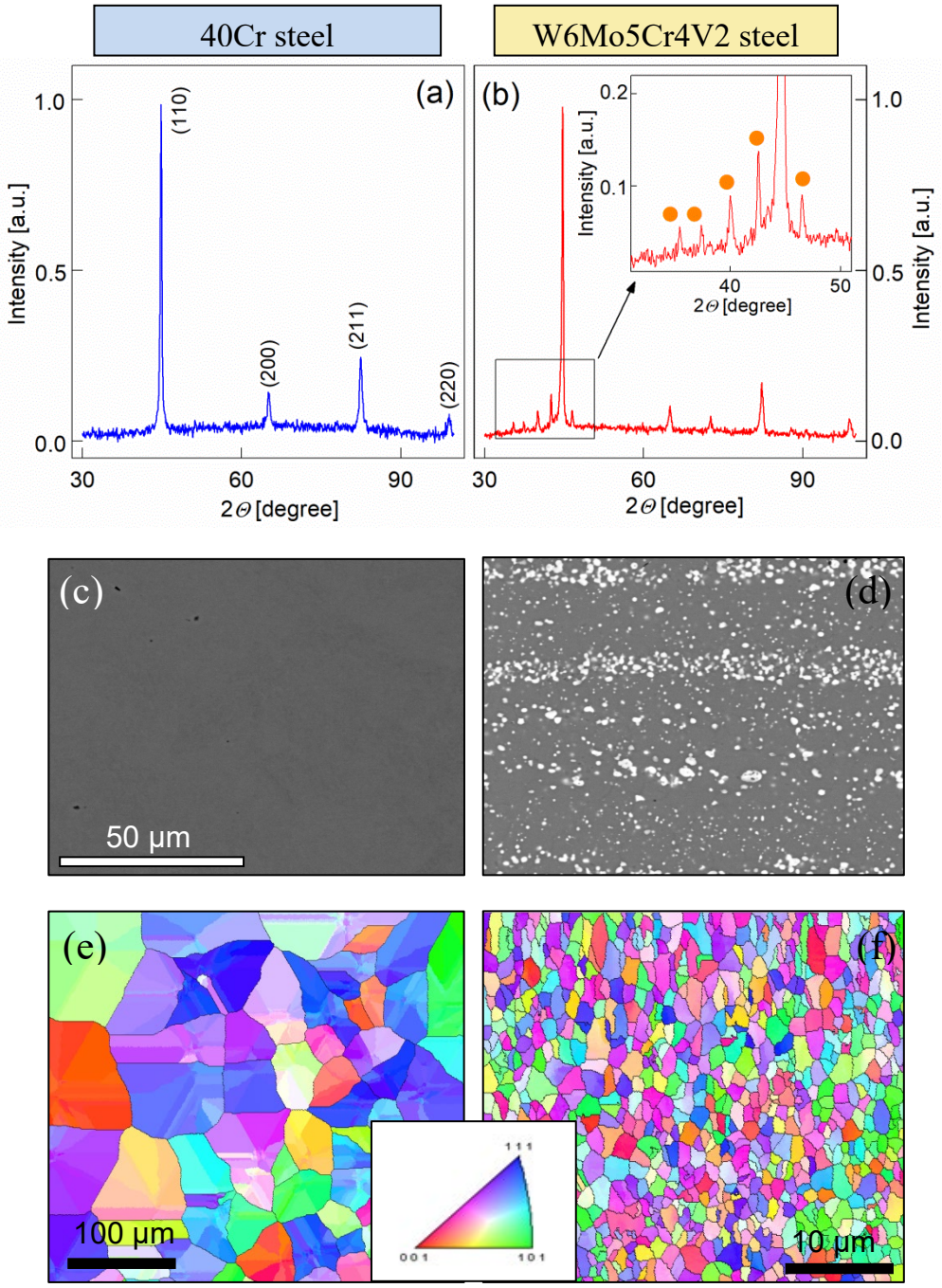

Fig. 1. XRD patterns ((a) and (b)), BSE-SEM images ((c) and (d)) and EBSD-SEM maps ((e) and (f)) taken for the 40Cr (left) and W6Mo5Cr4V2 (right) steels. Inset to Fig. (b) is large-scaled part of relevant XRD pattern that confirms forming the metal carbides (orange circle-shaped symbols correspond to the carbides phases). Inset to Figs. I and (f) shows a link between color of the grain and its crystallographic orientation.

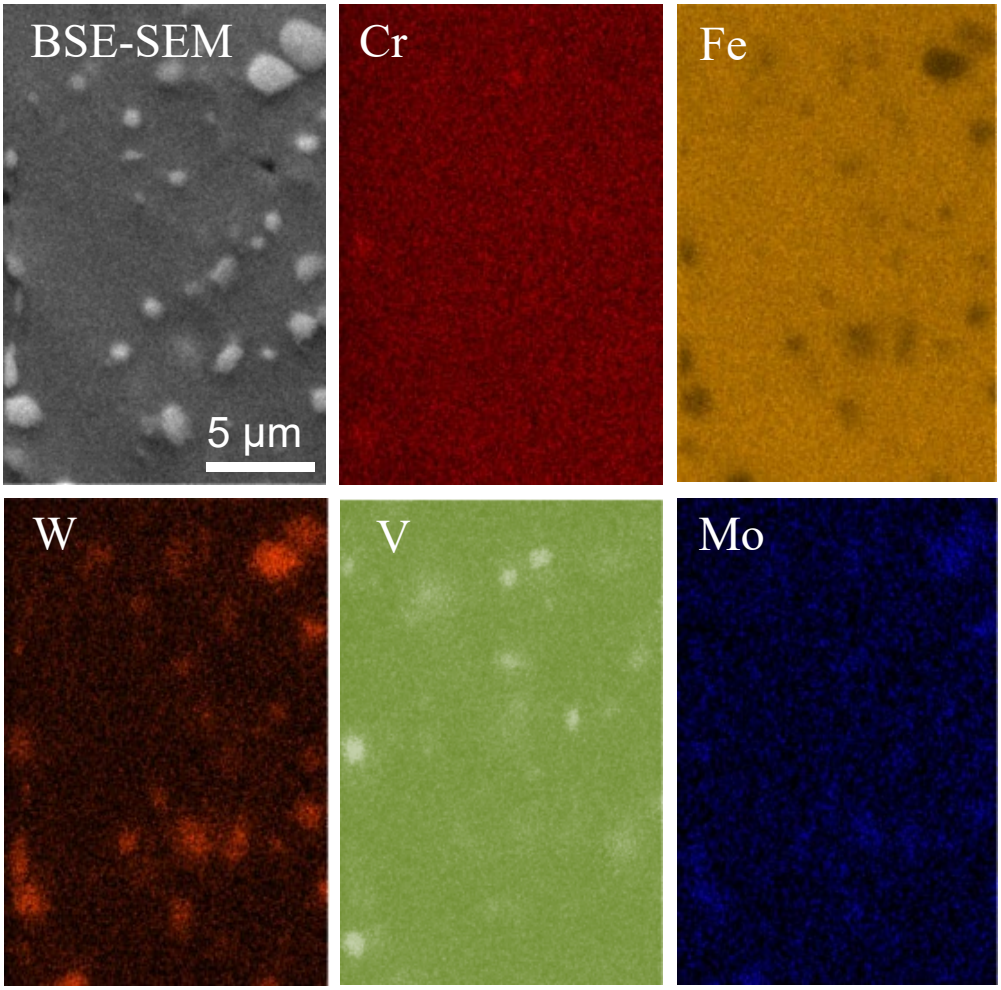

Fig. 2. BSE-SEM image taken from fractured surface of the W6Mo5Cr4V2 steel and distribution maps of Cr, Fe, W, V and Mo taken for this surface.

The BSE-SEM image of the 40Cr steel is presented by a homogeneous gray background and, hence, really corresponds to single-phased material. Several black islands, which are also observed in the BSE-SEM image, are pores forming during surface polishing. In contrast to the homogeneously colored BSE-SEM image for the 40Cr steel, light inclusions distributed inside the homogeneous gray background are clearly observed in the BSE-SEM image of the W6Mo5Cr4V2 steel. Therefore, this BSE-SEM image corresponds to multi-phased material. By comparing XRD patterns (**Figs. 1 (a)** and **(b)**) and BSE-SEM images (**Figs. 1 (c)** and **(d)**) taken for the 40Cr and W6Mo5Cr4V2 steels, the light inclusions should be attributed to the metal carbides forming only in the W6Mo5Cr4V2 steel. Forming the metal carbides inside the W6Mo5Cr4V2 steel is accompanied by relevant inhomogeneous distribution of different elements. BSE image and distribution maps of Cr, Fe, W, V and Mo taken from a fractured surface of the steel are shown in **Fig. 2**. As resulted from this Figure, inhomogeneties in the element distributions really correspond to the light inclusions in accordance with the BSE-SEM image. Visually, the most inhomogeneous distribution is observed for W, Fe and V. The light inclusions are W- and V-enriched, and Fe-deficient. As will be discussed below, these inclusions are Mo-enriched and Cr-deficient, too. The light carbides inclusions have irregular shape and size ranging from several hundreds of nanometers to several microns. These inclusions form elongated chains. Ordering the carbide inclusions is known to be characteristic of cold and hot rolled steels (Seol et al., 2013). Thus, the W6Mo5Cr4V2 steel can be considered as a composite material consisting of matrix phase based on Fe and filler inclusions corresponding to the metal carbides phases.

Besides the difference in the elemental and phase composition, the 40Cr and W6Mo5Cr4V2 steels are also different in their grain structure. To characterize the grain structure, EBSD-SEM maps were taken from thoroughly polished surfaces of the steels (**Fig. 1 (e)** and **(f)**). To take these maps, only high angle grain boundaries with angles ranging from 15 to 60° were taken into account. EBSD-SEM maps present a distribution of crystallographic orientations for surface grains. A colour of separate grains is directly connected with their crystallographic orientations in accordance with inset to Figure. EBSD-SEM maps allow visualizating the grain structure of grained material and estimate shape and size of the grains. As resulted from analysis of EBSD-SEM maps, the grain size is remarkably different in the 40Cr and W6Mo5Cr4V2 steels. The 40Cr steel is a coarse-grained alloy since it consists of big grains with average size of ~100 μm, whereas the W6Mo5Cr4V2 steel is fine-grained alloy consisting of small grains with average size of several μm. For both steels, the grains are irregularly-

shaped. Thus, the 40Cr steel is single-phased and coarse-grained alloy with homogeneous inclusions-less microstructure, and the W6Mo5Cr4V2 steel is multi-phased and fine-grained alloy with inhomogeneous composite microstructure consisting of matrix Fe-based phase with metal carbides filler distributed as inclusions chains inside the matrix.

3.2 Diffusion welding process between the 40Cr and W6Mo5Cr4V2 steels

Schematic of diffusion welding process between the 40Cr and W6Mo5Cr4V2 steels is presented in **Fig. 3**. The diffusion welding process consists of 4 stages.

Stage I corresponds to the initial state of the steels being welded. The 40Cr and W6Mo5Cr4V2 discs with treated contact surfaces were placed in a special holder, which is vacuum sealed and can be evacuated by a turbo molecular pump (**Fig. 4**). The distance between the upper 40Cr steel disc and bottom W6Mo5Cr4V2 steel disc was usually 3-4 mm. The holder with fixed discs was at room temperature and ambient pressure.

Stage II corresponds to preliminary high-temperature treatment of the 40Cr and W6Mo5Cr4V2 discs fixed in the holder. Before the high-temperature treatment, the holder was evacuated to 10^{-5} mbar and heated to 800 ºC, and then placed in a resistance furnace preliminary heated to 1200 ºC. The holder with fixed steel discs was kept at this temperature for one hour resulting in a preliminary high-temperature state.

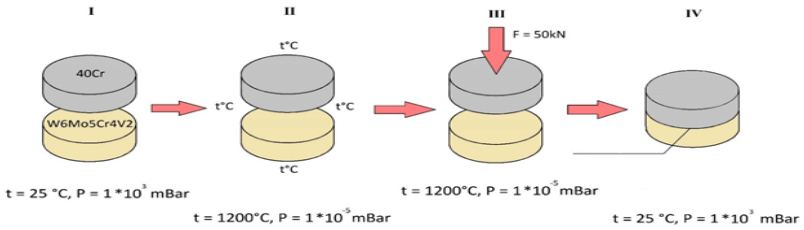

Fig. 3. Schematic of four-staged diffusion welding process between the 40Cr and W6Mo5Cr4V2 steels. Stage I is initial state of the steels, stage II is preliminary high-temperature state of the steels, stage III is applying the uniaxial compression to the steels in high-temperature state, and stage 4 is final state corresponding to the diffusion-welded steels.

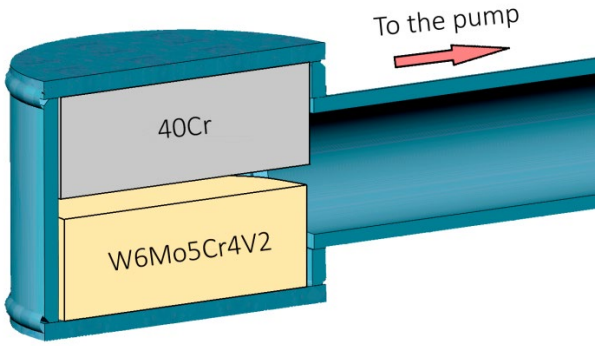

Fig. 4. Vacuum sealed holder for arrangement of the 40Cr and W6Mo5Cr4V2 discs applied for their diffusion welding.

Stage III corresponds to the uniaxial 50 kN compression of the steel discs in high-temperature state.

Stage IV corresponds to cooling the steel discs. Just after the uniaxial compression, the compression pressure was released, and the holder was naturally cooled from high-temperature state to room temperature in air atmosphere at ambient pressure finally resulting in forming the 40Cr-W6Mo5Cr4V2 joint.

3.3 Characterization of welding joint forming between the 40Cr and W6Mo5Cr4V2 steels

Diffusion welding of the 40Cr and W6Mo5Cr4V2 steels resulted in forming a narrow and sharp welding joint between the steels. BSE-SEM image and EBSD-SEM map taken for these steels are shown in **Fig. 5**.

The welding joint connecting the 40Cr and W6Mo5Cr4V2 steels to each other can be clearly observed in this Figure. According to BSE-SEM image, the microstructure features, which are characteristic for the initial 40Cr and W6Mo5Cr4V2 steels before their diffusion welding (**Fig. 1 ((e) and (d)**), are preserved in these steels after the diffusion welding, i.e. the 40 Cr steel microstructure is homogeneous and inclusions-less that is characteristic of single-phased alloy, whereas the W6Mo5Cr4V2 steel microstructure corresponds to the composite microstructure, which is characteristic of multi-phased alloy, and the metal carbides inclusions form chains inside the alloy matrix.

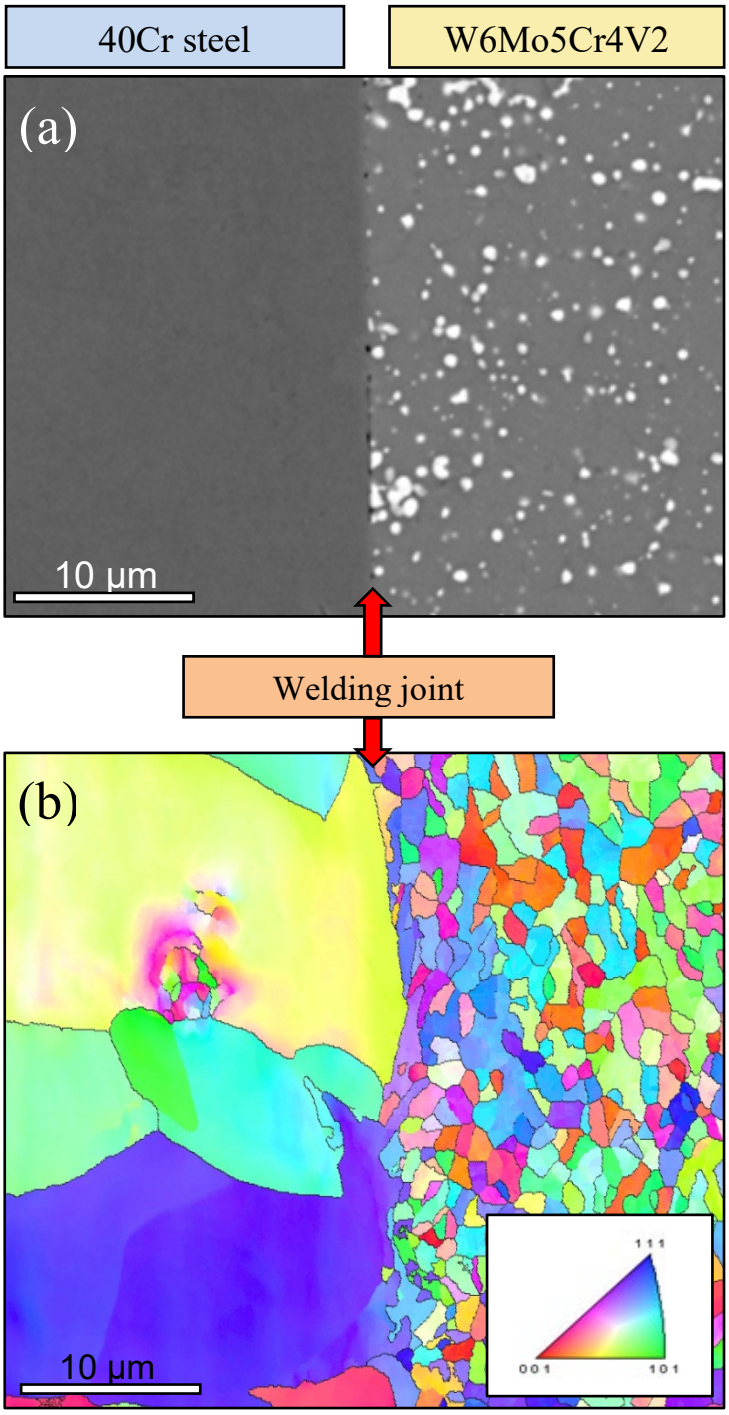

Fig. 5. BSE-SEM image (a) and EBSD-SEM map (b) taken for the diffusion-welded 40Cr and W6Mo5Cr4V2 steels. Inset to **Fig. (b)** shows a link between color of the grain and its crystallographic orientation.

The welding joint in the BSE-SEM image (**Fig. 5 (a)**) is almost straight between the left dark grey part corresponding to the 40Cr steel and the right light part corresponding to the W6Mo5Cr4V2 steel. No obvious changes in the grain structure of the coarse-grained 40Cr and fine-grained W6Mo5Cr4V2 steels after their diffusion welding can be also observed. The welding joint in the EBSD-SEM map is a broken line corresponding to contacts between the big grains in the 40Cr steel and the small grains in the W6Mo5Cr4V2 steel. Diffusion welding process is based on a high-temperature solid-state diffusion redistribution of atoms between the steels being welded. To characterize a distribution of different elements at/near the 40Cr-W6Mo5Cr4V2 joint, EDS line scan profiles of host Fe element and alloying Cr, V, W and Mo elements were taken along a line crossing the welding joint (**Fig. 6**). The BSE-SEM image of the surface of the diffusion-welded 40Cr and W6Mo5Cr4V2 steels applied to take EDS line scan profiles is also shown in **Fig. 6**. Intensity of the signal in this Figure is proportional to relevant element concentration. The diffusion redistribution of atoms for all the elements at a gradual transition through the welding joint is really observed. This redistribution is in qualitative accordance with the different elemental composition of the 40Cr and W6Mo5Cr4V2 steels (**Table 1**). Namely, at a transition from the W6Mo5Cr4V2 steel with low Fe content and enriched with

Cr, V, W and Mo to the 40Cr steel with high Fe content and lower Cr, V, W and Mo content, the Fe content is gradually increasing, whereas the Cr, V, W and Mo content is gradually increasing. It should be noted that the Fe diffusion is a self-diffusion process, whereas the other elements diffusion is an impure hetero-diffusion process. In the 40Cr steel, EDS scan line profiles are presented by smooth curves. However, in the W6Mo5Cr4V2 steel, these line profiles behave in a more complicated manner. In EDS scan line profiles taken for Fe, V, W and Mo, deviations from a background line resulting in forming the minima (for Fe) or maxima (for V, W and Mo) are observed. These deviations are formed when the EDS scan lines go through or near the metal carbide chains existing in the W6Mo5Cr4V2 steel. As a result, these carbides locally contribute to the different element distribution for this steel. So, rather complicated behavior in these lines combining the carbides response and the matrix material response should be attributed to the composite microstructure of this steel.

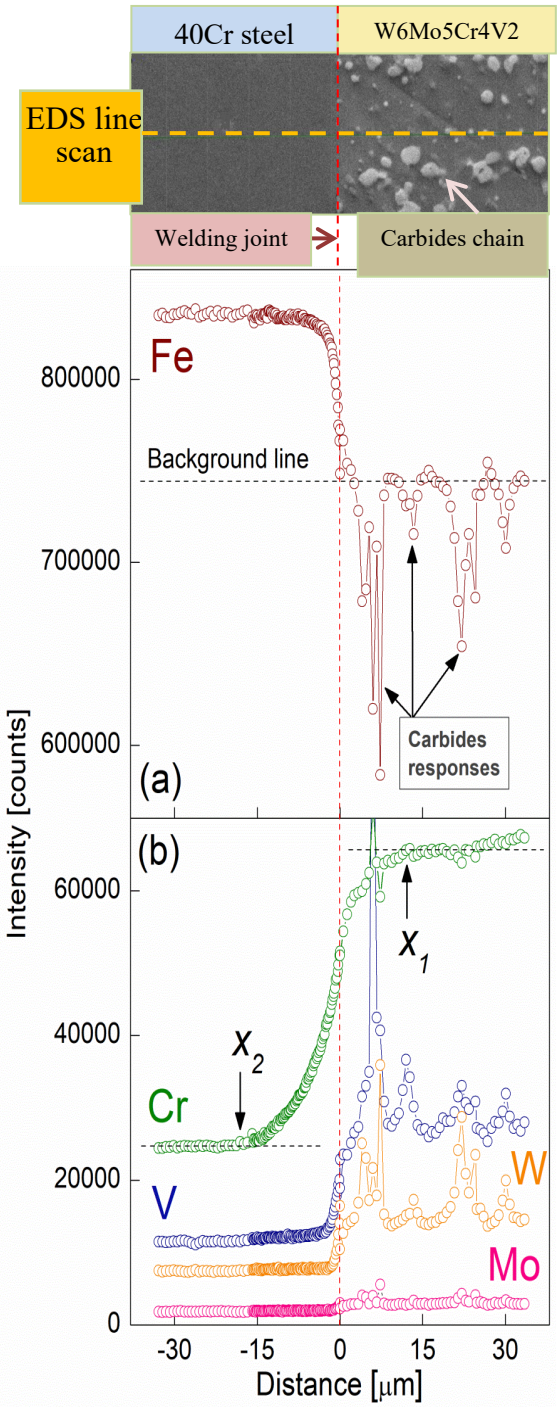

Fig. 6. BSE-SEM image of the diffusion-welded 40Cr and W6Mo5Cr4V2 steels and EDS scan lines profiles of host Fe element (a) and alloying Cr, V, W and Mo elements (b) taken along line crossing the welding joint.

Expectedly, the maxima in the V, W and Mo distributions are related to enhanced content of these elements inside the carbides inclusions. The maxima in the V and W distributions are the most pronounced, whereas the Mo maxima are much less pronounced. Positions of all the maxima observed for different elements coincide with each other. In contrast to alloying

V, W and Mo elements, the well-defined pronounced minima in host Fe distribution and the weakly defined minima in alloying Cr distribution were observed. These features are related to the fact that Fr and Cr are not involved in formation of the metal carbides.

Diffusion redistributions of Fe, Cr, V, W and Mo atoms between the 40Cr and W6Mo5Cr4V2 steels, which are shown in **Fig. 6**, are limited with a spatial interval between two points X_1 and X_2, where X_1 is point in the W6Mo5Cr4V2 steel and X_2 is point in the 40Cr steel. At $x>X_1$ and $x<X_2$ homogeneous distribution of the atoms takes place (x is a direction perpendicular to diffusion welding plane). For instance, the X_1 and X_2 points for Cr distribution are shown in Fig. 6 (b). Spatial $X_2<x<X_1$ interval corresponds to a diffusion zone for atoms being diffused. One can see that (i) the diffusion zones for all the elements are non-symmetric regarding the welding joint, since they are shifted to the 40Cr steel, and (ii) the width of the diffusion zone is different for different atoms being diffused. Maximal width equal to ~25 μm is observed for the diffusion Cr zone. As result, a rather smooth change in Cr distribution is formed during the diffusion welding. The diffusion Fe zone is ~15 μm, and the diffusion V, W and Mo zones are remarkably narrower as compared to Cr and Fe, and equal to several μm. As result, a sharp step-like change in V, W and Mo distributions takes place within the relevant diffusion zones.

Different width of the diffusion zones for Fe, Cr, V, W and Mo atoms is obviously originated from difference in a penetration depth for these atoms. In accordance with the Fick's first law, a diffusion movement of atoms from high to low concentration (diffusion flux, $\vec{J}$) is directly proportional to an atoms concentration gradient. For one spatial dimension, this law can be written as

$$\vec{J} = -D\frac{dC}{dx}, \quad (1)$$

where D is the diffusion coefficient for atoms being diffused, C is the atoms concentration, and dC/dx is the concentration gradient along x-direction

For diffusion of Fe, Cr, V, W and Mo atoms during the diffusion welding between the 40Cr and W6Mo5Cr4V2 steels, relevant concentration gradients should be determined by difference in elemental composition of these steels (**Table 1**). According to **Table 1**, the highest concentration gradients are found namely for V, W and Mo. However, the diffusion zones for these elements are narrower as compared to Cr and Fe. In contrast to Cr and Fe, V, W and Mo form the metal carbides in the W6Mo5Cr4V2 steel, i.e. part of atoms of these elements with their concentration listed in Table 1 are chemically-bounded in the carbides. These metal carbides cannot act as diffusion sources for V, W and Mo diffusion. Therefore, only atoms that are not part of the carbides can participate in the diffusion processes. As result, real concentration gradients for these elements could be much smaller than that formally determined from difference in the element concentrations, not taking into account the specific composite microstructure of the W6Mo5Cr4V2 steel. Decreasing in real concentration gradients for V, W and Mo atoms in comparison with Cr and Fe atoms could be responsible for the difference in width of the relevant diffusion zones. Besides, the diffusion coefficients for Cr, Fe, V, W and Mo atoms can be different, too. Rather broad diffusion Cr zone corresponding to smooth enough change in Cr content can be applied to examine Cr diffusion during the diffusion welding of the 40Cr and W6Mo5Cr4V2 steels (Fig. 6 (a)). By using EDS scan lines profile for Cr, a concentration $C(x)/C_0$ profile was plotted in **Fig. 7** (concentration C_0 corresponds to X_1=0 point, and concentration $C(x)$ is x-dependent concentration at x-changes from X_1 to X_2). This profile is typical for atomic diffusion from a limited source (Zhezhu et al., 2024). For this diffusion type, the concentration $C(x)$ profile, which is formed in time t, will obey expression (Poirier & Geiger, 2016).

$$C(x,t) = C_0 exp[-x^2/\omega^2], \quad (2)$$

where $\omega = \sqrt{4Dt}$ is the T- and t-dependent parameter.

Expression (2) is a solution of the Fick's second law

$$\frac{dC}{dt} = D\frac{d^2C}{d^2x}. \quad (3)$$

Typically, a diffusion coefficient, D, depends on temperature in accordance with the Arrhenius law

$$D = D_0 exp[-E_a/k_B T], \quad (4)$$

where k_B is the Boltzmann's constant, E_a is the activation energy of diffusion process and D_0 is the pre-exponential factor.

Actually, expression (2) can be satisfactory applied to fit the experimental $C(x)/C_0$ versus x dependence for Cr diffusion, as is shown by solid red curve in **Fig. 7**.

The fitting ω parameter was extracted as ~11.7 μm. To form a desired concentration profile for atom diffusion, relevant diffusion process is usually implemented at a constant temperature and a constant holding time. In this case, fitting procedure

of the concentration profile by expression (2) allows estimating the relevant diffusion coefficient. However during the diffusion welding of the 40Cr and W6Mo5Cr4V2 steels, atom diffusion occurs within a broad temperature range corresponding to cooling the uniaxially compressed 40Cr and W6Mo5Cr4V2 discs from maximal 1200 ºC temperature to room temperature. In accordance with expression (4), the diffusion coefficient will correspond to each temperature from this temperature range. Therefore, resulting concentration profile for atoms being diffused, which is formed after completion of diffusion process, will be determined by combination of numerous diffusion processes with various T-dependent diffusion coefficients. Dependence of welding temperature, T_w, versus welding time, t_w, taken for the diffusion welding between the 40Cr and W6Mo5Cr4V2 steels is shown in **Fig. 8**.

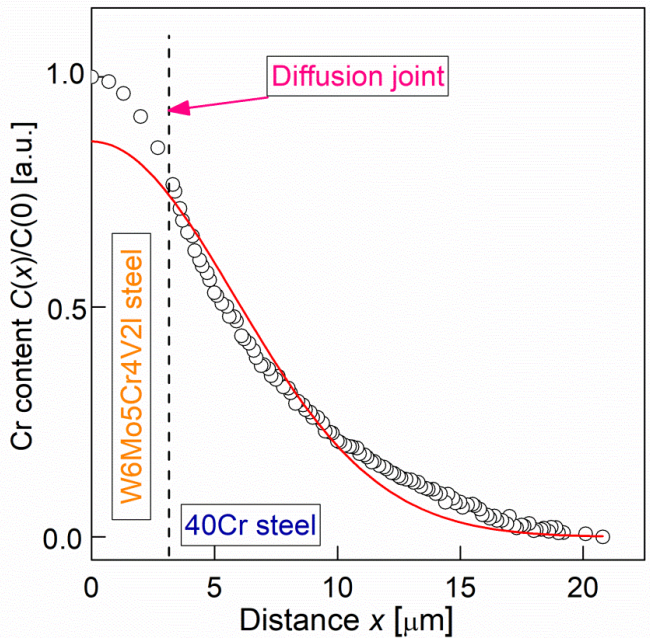

Fig. 7. Concentration Cr profile formed after completion of the diffusion welding of the 40Cr and W6Mo5Cr4V2 steels. Solid red curve is the fitting one.

For 50 min, the T_w decreases from 1200 ºC to 40 ºC. By using the values $\omega \approx 11.7$ μm and t_w=50 min, the diffusion coefficient for atoms Cr was estimated as ~$1.1 \cdot 10^{-14}$ $m^2 \cdot s^{-1}$. This coefficient D_{Cr}^{w} should be considered as weighted over the entire temperature range corresponding to diffusion Cr embedding from the W6Mo5Cr4V2 steels into the 40Cr steel. The weighted D_{Cr}^{w} coefficient value estimated for Cr diffusion in the W6Mo5Cr4V2 steel is close to the diffusion coefficient for Cr diffusion in Fe-Cr alloy and α-Fe lattice diffusion at ~930 ºC (Wang et al., 2006).

3.4 Mechanical properties of the diffusion welded 40Cr and W6Mo5Cr4V2 steels

To characterize the mechanical properties of the diffusion-welded 40Cr and W6Mo5Cr4V2 steels, the Vickers microhardness profiles at/near the welding joint and the room-temperature engineering strain-stress curves were recorded.

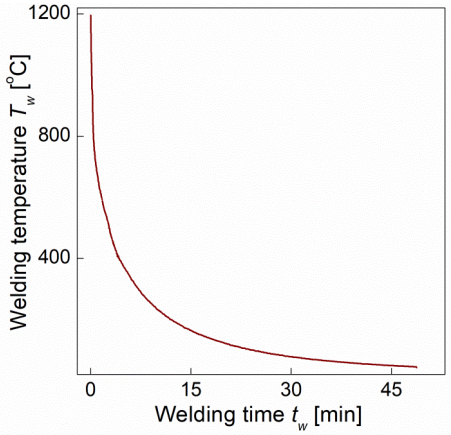

Fig. 8. Dependence of welding temperature T_w versus welding time t_w during the diffusion-welding between the 40Cr and W6Mo5Cr4V2 steels.

The Vickers microhardness profile taken at 22 mN is shown in **Fig. 9 (a)**. In side of the W6Mo5Cr4V2 steel, experimental points are scattered around the ~2000 HV value that corresponds to the Vickers microhardness of this steel. The scattering in experimental data can be attributed to the composite microstructure of the steel consisting of the Fe-based matrix and the different metal carbides inclusions. Owing to this microstructure, the surface microhardness will depend on the material (matrix material or metal carbides material) at the indentation site.

At a transition from the W6Mo5Cr4V2 steel to the 40Cr steel, the Vickers microhardness gradually decreases trending to the ~530 HV value characteristic for the 40Cr steel. In side of the 40Cr steel, change in the microhardness corresponds to the diffusion Cr and Fe zones. As is shown at instance for Cr in **Fig. 9 (b)**, the microhardness change is in satisfactory agreement with change in Cr content within the relevant diffusion zone, i.e. decrease in Cr content is accompanied by decrease in the Vickers microhardness.

Step-like change in the microhardness observed across the welding joint for the diffusion-welded 40Cr and W6Mo5Cr4V2 steels is typical for other diffusion-welded dissimilar materials, including the diffusion-welded 304L/Monel K-500 steels (Kejanli, 2020), AISI 4140 and AISI 304 steels (Khedr et al., 2023), and the dissimilar Cu-Fe, Cu-Ag, Cu-Al and Al-Ni metals (Tsakiris et al., 2011), etc.

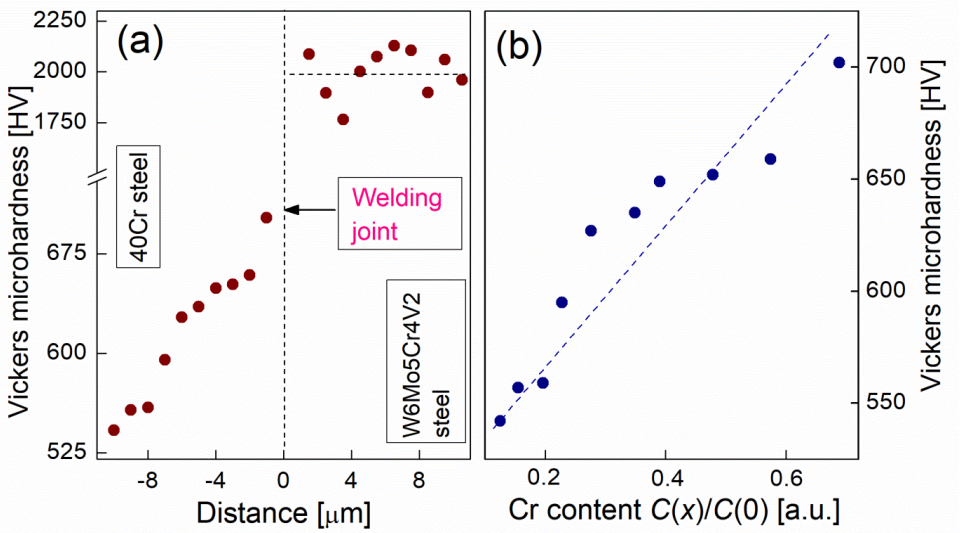

Fig. 9. (a) Dependence of the Vickers microhardness versus distance from the welding joint for the diffusion-welded 40Cr and W6Mo5Cr4V2 steels, and (b) dependence of the Vickers microhardness versus Cr content taken within the diffuse Cr zone. Dashed line is drawn as guides to the eyes.

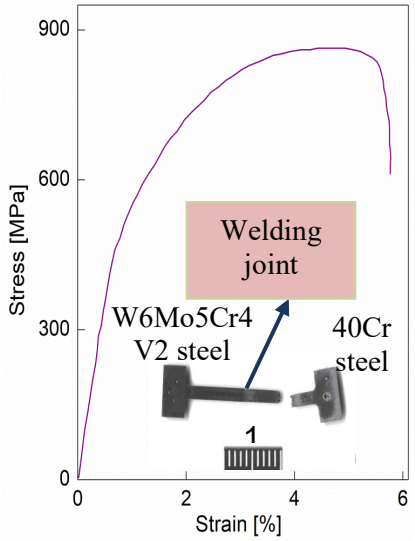

Fig. 10. Engineering strain-stress curve for the diffusion-welded 40Cr and W6Mo5Cr4V2 steels and photograph of the fractured sample.

o characterize a tensile behavior of the diffusion-welded 40Cr and W6Mo5Cr4V2 steels, the room-temperature engineering strain-stress curves were recorded for 5 different samples. One of these curves is shown in **Fig. 10**. Photograph of the fractured sample applied to take this curve is also shown in figure. All the samples always failed in the 40Cr steel.

Therefore, the mechanical strength of the diffusion joint is at least higher than the strength of this steel. Analysis of the engineering strain-stress curves allowed extracting the yield strength (YS), ultimate tensile strength (UTS) and total elongation (TE) the diffusion-welded 40Cr and W6Mo5Cr4V2 steels. For all the samples applied for tensile testing these values were close to each other. For instance, the curve in Fig. 10 is characterized by YS≈455 MPa, UTS≈850 MPa and TE≈5.75 %. These YS and UTS values are in accordance with mechanical properties of the commercial W6Mo5Cr4V2 steel. For instance, one of the products produced by a company SteelGr - China steel suppliers is the W6Mo5Cr4V2 steel with YS ranging from 350 to 550 MPa and UTS ranging from 650 to 880 MPa (Company SteelGr - China steel suppliers).

4. Conclusion

The main results extracted from detailed examination of bot diffusion welding process applied to the dissimilar structural 40Cr and high-speed tool W6Mo5Cr4V2 steels and the properties of the diffusion-welded steels are listed as follows:

(i) No obvious changes in the grain structure of the 40Cr and W6Mo5Cr4V2 as well as in the composite microstructure of the W6Mo5Cr4V2 steel were observed both near and apart from the welding joint.

(ii) Diffusion redistribution of host Fe atoms and alloying Cr, W, V, Mo atoms occurred during the diffuse welding between the steels. The diffusion V, W and Mo zones equal to several μm are remarkably narrower as compared to the diffuse Cr and Fe zones equal to ~25 and ~15 μm, respectively.

(iii) Owing to the composite microstructure of the W6Mo5Cr4V2 steel, only part of atoms V, W and Mo, which are not chemically-bounded in the relevant carbides, can diffuse from the W6Mo5Cr4V2 steel in the 40Cr steel.

(iv) The concentration Cr profile formed as result of diffusion processes with various and T-dependent diffusion coefficients is typical for the diffusion from the limited source. This profile can be satisfactorily described by one diffusion coefficient equal to $\sim 1.1 \cdot 10^{-14}$ $m^2 \cdot s^{-1}$ that is weighted over the entire temperature range corresponding to the diffuse welding.

(v) At gradual transition through the diffusion joint from the W6Mo5Cr4V2 steel into the 40Cr steel, the Vickers microhardness naturally decreases from ~2000 HV (for W6Mo5Cr4V2) to ~530 HV (for 40Cr). This microhardness behavior is in accordance with decrease of Cr content.

(vi) As resulted from the tensile test, the mechanical strength of the diffusion joint is at least higher than the strength of the 40Cr steel, since the samples of the diffusion-welded 40Cr and W6Mo5Cr4V2 steels always failed in the 40Cr steel.

Acknowledgements

All of the studies were carried out by the scientific equipment of the joint research center “Technologies and Materials” at the Belgorod State University.

References

Akca, E., & Gürsel A. (2016). Solid state welding and application in aeronautical industry, *Periodicals of Engineering & Natural Sciences*, *4*(1).

Akca, E., & Gursel, A. (2017). The effect of diffusion welding parameters on the mechanical properties of titanium alloy and aluminum couples. *Metals*, *7*(1), 22.

Akhter, J., Ahmad, M., Iqbal, M., Akhnar, M., & Shaikh, M.A. (2005). Formation of dendritic structure in the diffusion zone of the bonded Zircaloy-4 and stain less steel 316L in the presence of Ti interlayer. *Journal of Alloys & Compounds*, *399*(1-2), 96-100.

Anawa, E.M., & Olabi, A.G. (2008). Control of welding residual stress for dissimilar laser welded materials. *Journal of Materials Processing Technology, 204*, 22-33.

Baskutis, S., Baskutiene, J., Bendikiene, R., Ciuplys, A., & Dutkus, K. (2021). Comparative research of microstructure and mechanical properties of stainless and structural steel dissimilar welds. *Materials*, *14*(20), 6180.

Company SteelGr - China steel suppliers. https://www.steelgr.com/Steel-Grades/Tool-Steel-Hard-Alloy/w6mo5cr4v2.html .

Coronado, J., & Cerón, C. (2010). Fracture mechanisms of CTOD samples of submerged and flux cored arc welding. *Theoretical & Applied Fracture Mechanics*, *53*(2), 145-151

Chen, S., Liu, X., Lei, J., Zhu, L., & Wang. T. (2023). Boosting mechanical properties of W6Mo5Cr4V2 alloy fabricated by directed energy deposition through tempering heat treatment. *Steel Research International*, *94*(12).

Ghosh, N., Pal, P.K., & Nandi, G. (2017). GMAW dissimilar welding of AISI 409 ferritic stainless steel to AISI 316L austenitic stainless steel by using AISI 308 filler wire. *Engineering Science & Technology, an International Journa*l, *20*(12), 1334-1341.

Gietzelt, T., Toth, V., & Huell, A. (2018). Challenges of diffusion bonding of different classes of stainless steels. *Advanced Engineering Materials, 20*.

Gómez de Salazar, J.M., Barrena, M.I., Merino, N., & Matesanz, L. (2006). Diffusion welding of WC-Co (hardmetal)/high strength steels. *Materials Science Forum, 514-516*, 1526-1530.

Harada, Y., Sada, Y., & Kumai, S. (2014). Dissimilar joining of AA2024 aluminum studs and AZ80 magnesium plates by high-speed solid-state welding. *Journal of Materials Processing Technology, 214*, 477-484.

Hwang, J.-B., Sa, I., Kim, E.-S., & Lee, D.-H. (2023). Diffusion Welding of Surface Treated Alloy 800H. *Metals*, *13*(10), 1727.

Kazakov, N.F. (1985). *Diffusion Bonding of Materials*. Elsevier.

Kejanli, H. (2020) Diffusion welding of stainless steel 304L/Monel K-500 composite materials produced with different methods. *Advanced Composites Letters*, *29*, 1-10.

Khedr, M., Hamada, A., Järvenpää, A., Elkatatny, S., & Abd-Elaziem, W. (2022). Review on the solid-state welding of steels: diffusion bonding and friction stir welding processes. *Metals*, *13*(1), 54.

Kurt, B. (2007). The interface morphology of diffusion bonded dissimilar stainless steel and medium carbon steel couples. *Journal of Materials Processing Technology*, *190*(1-3), 138-141.

Li, S., Xuan, F., Tu, S., & Yu, S.R. (2008). Microstructure evolution and interfacial failure mechanism in 316LSS diffusion-bonded joints. *Materials Science and Engineering A-structural Materials Properties Microstructure and Processing, 491*, 488-491.

Mahoney, M.W., & Bampton, C.C. (1993). *Fundamentals of Diffusion Bonding, Brazing and Soldering*. ASM Handbook-Welding.

Nassiri, A., Abke, T., & Daehn, G. (2019). Investigation of melting phenomena in solid-state welding processes. *Scripta Materialia*, *168*, 61-66.

Qu, M., Wang, Z., Li, H., Lv, Z., Sun, S., & Fu W. (2013). Effects of mischmetal addition on phase transformation and as-cast microstructure characteristics of M2 high-speed steel. *Journal of Rare Earths*, *31*(6), 628-633.

Poirier, D.R., & G.H. Geiger (2016). *Transport Phenomena in Materials Processing*. Springer.

Seol, J.-B., Raabem, D., Choi, P.-P., Park, H.-S., Kwak, J., & Park, C.-G. (2013). Direct evidence for the formation of ordered carbides in a ferrite-based low-density Fe–Mn–Al–C alloy studied by transmission electron microscopy and atom probe tomography. *Scripta Materialia*, *68*, 348-353.

Sharma, G., & Kumar Dwivedi, D. (2021). Diffusion bonding of 304 austenitic stainless-steel using pressure pulses. *Materials Today: Proceedings*, *44*(1-2), 2135-2141.

Senthur Vaishnavan, S., & Jayakumar, K. (2021). Tungsten inert gas welding of two aluminum alloys using filler rods containing scandium: the role of process parameters. *Materials and Manufacturing Processes, 37*, 143-150.

Singh, D.K., Sharma, V., Basu, R., & Escandari, M.. (2019). Understanding the effect of weld parameters on the microstructures and mechanical properties in dissimilar steel welds. *Procedia Manufacturing*, *35*, 986-991.

Takeda, T., Kunitomi, K., Horie, T., & Iwata, K. (1997). Feasibility study on the applicability of a diffusion-welded compact intermediate heat exchanger to next-generation high temperature gas-cooled reactor. *Nuclear Engineering & Design*, *168*(1-3), 11-21.

Tsakiris, V., Kappel, W., & Alecu, G. (2011). Solid state diffusion welding of Cu-Fe/Al/Ag and Al-Ni dissimilar metals. *Journal of Optoelectronics & Advanced Materials*, *13*(9), 1176-1180.

Tümer, M., Schneider-Bröskamp, C., & Enzinger, N. (2022). Fusion welding of ultra-high strength structural steels – A review. *Journal of Manufacturing Processes*, *82*, 203-229.

Wang, J., Li, Y., & Huang, W. (2008). Interface microstructure and diffusion kinetics in diffusion bonded Mg/Al joint. *Reaction Kinetics & Catalysis Letters*, *95*, 71-79.

Wang, Z.B., Tao, N.R., Tong, W.P., Lu, K., Philibert, J., & Beke, D. (2006). Diffusion of Cr in nanostructured Fe and low carbon steel produced by means of surface mechanical attrition treatment. *Defect & Diffusion Forum*, *249*, 147-154.

Yao, Y., Xiu, S., Sun, C., Kong, X., & Hong, Y. (2021). Investigation on grinding-induced dynamic recrystallization behavior of 40Cr alloy steel. *Journal of Alloys & Compounds*, *867*(18).

Yildirim, S., & Kelestemur, M.H. (2005). A study on the solid-state welding of boron-doped Ni_3Al–AISI 304 stainless steel couple. *Materials Letters*, *59*(10), 1134-1137.

Yılmaz, O. (2001). Effect of welding parameters on diffusion bonding of type 304 stainless steel–copper bimetal. *Materials Science & Technology*, *17*(8), 989-994.

Yin, P., Zang, H., Zhao, Y., Wu, C., Xu, X., Pan, D., & Jiang, W. (2020). Superior mechanical properties of 40Cr steel obtained by quenching and microstress relieving under electropulsing. *Materials Science and Engineering A-structural Materials Properties Microstructure and Processing, 772*, 138782.

Xiong, J., Peng, Y., Samiuddin, M., & et al. (2020). Common mechanical properties of diffusion bonded joints and their corresponding microstructure features. *Journal of Materials Engineering & Performance*, *29*(5), 3277-3286

Zhang, C., Li, H., & Li, M. (2015). Formation mechanisms of high quality diffusion bonded martensitic stainless steel joints. *Science and Technology of Welding & Joining*, *20*(2), 115-122.

Zhezhu, M., Vasil'ev, A., Ivanov, O., & et al. (2024). Effects of locally-gradient Co-doping on the electron properties of $Bi_2Te_{2.1}Se_{0.9}$ + 0.33 wt.% Co composite. *Materialia*, *36*, 102172.